Two-dimensional ferroelectric topological insulators in functionalized atomically thin bismuth layers

Liangzhi Kou, Huixia Fu, Yandong Ma, Binghai Yan, Ting Liao, Aijun Du, and Changfeng Chen

Two-dimensional ferroelectric topological insulators in functionalized atomic thin bismuth layers

Liangzhi Kou[1*], Huixia Fu[2], Yandong Ma[3], Binghai Yan[2], Ting Liao[1], Aijun Du[1] & Changfeng Chen[4]

[1]*School of Chemistry, Physics and Mechanical Engineering Faculty, Queensland University of Technology, Garden Point Campus, QLD 4001, Brisbane, Australia*

[2] *Department of Condensed Matter Physics, Weizmann Institute of Science, Rehovot, 7610001, Israel*

[3] *School of Physics, State Key Laboratory of Crystal Materials, Shandong University, Shandanan Str. 27, 250100 Jinan, People's Republic of China*

[4] *Department of Physics and Astronomy and High Pressure Science and Engineering Center, University of Nevada, Las Vegas, Nevada 89154, United States*

Liangzhi.kou@qut.edu.au

We introduce a class of two-dimensional (2D) materials that possess coexisting ferroelectric and topological insulating orders. Such ferroelectric topological insulators (FETIs) occur in noncentrosymmetric atomic layer structures with strong spin-orbit coupling (SOC). We showcase a prototype 2D FETI in an atomic thin bismuth layer functionalized by CH_2OH, which exhibits a large ferroelectric polarization that is switchable by a ligand molecule rotation mechanism and a strong SOC that drives a band inversion leading to the topological insulating state. An external electric field that switches the ferroelectric polarization also tunes the spin texture in the underlying atomic lattice. Moreover, the functionalized bismuth layer exhibits an additional quantum order driven by the valley splitting at the K and K' points in the Brillouin zone stemming from the symmetry breaking and strong SOC in the system, resulting in a remarkable state of matter with the simultaneous presence of the quantum spin Hall and quantum valley Hall effect. These novel phenomena are predicted to exist in other similarly constructed 2D FETIs, thereby offering a unique quantum material platform for discovering novel physics and exploring innovative applications.

I. Introduction

Recent years have seen the rise of a distinct class of materials that exhibit topologically protected helical metallic edge states while maintaining an insulating bulk, leading to the so-called quantum spin Hall effect (QSHE)[1,2]. The remarkable properties of these topological insulators (TIs) provide a platform to elucidate fundamental physics principles underlying the new phenomena and explore innovative applications [3,4]. Of particular interest among these new quantum states of matter is a large family of two-dimensional (2D) TIs.[5-14] The strong spin-orbit coupling (SOC) in these materials provides the driving force for topological phase transitions; it also lifts the band degeneracy and leads to a spin splitting in inversion-asymmetric systems[15], producing the celebrated Rashba effect[16,17] that has traditionally been studied in surfaces and interfaces[18], and recently in the layered material BiTeI[19,20].

Ferroelectricity is an intriguing quantum phenomenon in materials possessing switchable spontaneous polarization. In insulators with strong SOC and inversion asymmetry in the crystal structures, interesting ferroelectric Rashba behaviour can be observed [21-23], where the spin texture can be reversed accompanying the ferroelectric switch[24,25]. Recent studies of GeTe[22] and tin iodide perovskite (FA)SnI_3[26] have shown that the combination of ferroelectricity and SOC leads to a giant Rashba effect with a tunable spin texture via ferroelectric switch [27]. These so called ferroelectric Rashba semiconductors (FERSC)[27] have been also found in ABC hyper-ferroelectrics (A=Li, Na, K; B=Be, Mg, Ca; C=Sb, Bi)[21,23,28]. While FERSCs are normal semiconductors, the associated findings raise the intriguing prospects of having SOC induced band inversion to accompany the ferroelectric polarization in some properly constructed materials. The coexistence of ferroelectricity and band topology in insulators can occur when SOC is strong enough to induce band inversion in materials that possess spontaneous charge polarization. Such materials have been identified by two groups that reported on computational discovery of 3D ferroelectric or antiferroelectric TIs in $CsPbI_3$[29] or orthorhombic AMgBi (A=Li, Na, K) compounds[28].

Recent studies have unveiled several 2D ferroelectric materials, including oxidized MXene (Sc_2CO_2)[30], SnS [31], and In_2Se_3 [32,33]. These 2D systems are highly desirable for their suitability for integration into device design and implementation, and exploration of possible multiple quantum orders in such materials would open new avenues for fundamental research and practical applications. In the letter, we showcase the coexistence of ferroelectric and band topological orders in a 2D functionalized bismuthene. The strong intrinsic SOC in Bi combined with a ligand induced structural asymmetry in functionalized bismuthene renders this system the first 2D ferroelectric TI (FETI). The resulting ferroelectricity is

controllable and switchable by a ligand molecule rotation mechanism with a low energy barrier of 0.12 eV. A large spin splitting is induced by the out-of-plane polarization from the structural symmetry breaking, leading to a quantum valley Hall effect at two non-equivalent K points. The helical spin texture is reversed upon the ferroelectric switch, similar to the results found in FERSCs. These findings make 2D FETIs promising candidates for spintronic applications.

II Methods

Structural relaxation and electronic structure calculations were carried out using first-principles methods based on the density functional theory (DFT) as implemented in the Vienna Ab Initio Simulation (VASP) package.[34] The generalized gradient approximation (GGA) in the Perdew–Burke–Ernzerhof (PBE)[35] form for the exchange and correlation potential, together with the projector-augmented wave (PAW) method, were adopted. The structural model for functionalized bismuthene is periodic in the x–y plane and is separated by at least 10 Å along the z-direction to avoid interactions between adjacent layers. All atoms in the unit cell were fully relaxed until the force on each atom is less than 0.01 eV Å^{-1}. The Brillouin zone integration was sampled by 11 × 11 × 1 k-grid mesh for a unit cell, which results in good convergence in calculated total energy. An energy cutoff of 400 eV was chosen for the plane wave basis. The van der Waals interaction was described by a semiempirical correction using the Grimme method (DFT-D3)[36]. Spin–orbit coupling (SOC) was included at the second variational step using scalar-relativistic eigenfunctions as a basis. The macroscopic electric polarization of the system is calculated using the Berry phase method, which includes both the ionic and electronic contributions. Energy barriers for phase transitions were calculated using the climbing-image nudge elastic band (CI-NEB) method as implemented in the VASP transition state tools[37]. We have used eight images for energy barrier calculations between two phases, including initial and final positions. The maximally localized Wannier functions (MLWFs) are constructed using the WANNIER 90 code within VASP for Z_2 calculations.

III Results and Discussion

Ligand CH_2OH functionalized bismuth monolayer (short for B-CH_2OH) is chosen as a prototype 2D FETI to showcase the main characteristics and elucidate the underlying mechanisms. Very recently a 2D bismuth honeycomb lattice was synthesized on top of a SiC substrate[14], it exhibits a nontrivial gap of 0.8 eV. Surface functionalization of bismuthene

using small functional groups (H, F, Cl, Br) further raises the gap to 1 eV [10,38]. This large gap provides a stable platform for ferroelectric order in the system by avoiding a macroscopic depolarization caused by the metallization stemming from temperature or environmental conditions[39]. While ligand functionalized bismuthene is yet to be realized experimentally, there has been report on covalently functionalized germanane by ligand groups CH_2OCH_3, CH_3 and CH_2CHCH_2 [40,41], which provides guidance for the functionalization of bismuthene using similar ligand groups. Even so, it remains as a challenge to precisely synthesize ligand functionalized bismuthene in experiments, the current model is mainly used as a theoretical model to demonstrate the coexistence of ferroelectricity and Quantum Spin Hall effect in a single 2D material, but expected to be verified experimentally.
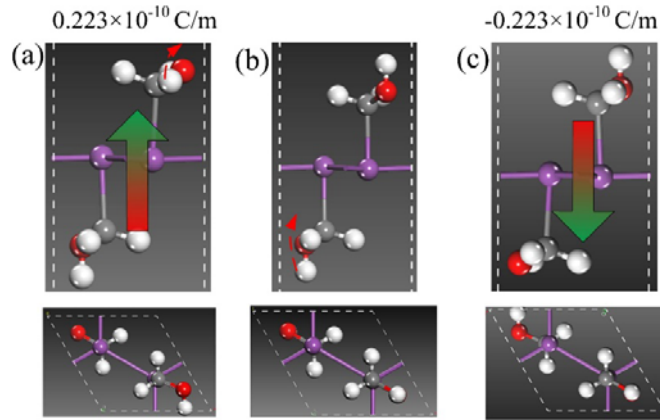

Figure 1. Side (upper row) and top (lower row) views of Bi-CH$_2$OH with (a-c) positive, zero and negative out-of-plane polarization. The purple, grey, red and white balls represent Bi, C, O and H atoms, respectively. The thick arrows indicate the polarization directions, and the thin dashed-curve arrows indicate the H-atom rotation that switches the ferroelectric polarization from pointed up (a) to neutral (b) to pointed down (c).

Fig. 1 presents the relaxed structure of Bi-CH$_2$OH in different configurations, where the Bi atoms adopt a stable sp^3 state with the chemical functional groups bonding on both sides of the plane in an alternating way. The paraelectric phase shown in Fig. 1b possesses inversion symmetry with point group D_{3d}, therefore exhibiting no spontaneous electric polarization. However, the symmetric configuration is not the most energetically stable. When the H atom of hydroxide on one side is rotated, a more stable configuration is obtained (Fig. 1a) while the ligand CH$_2$OH on the opposite side remains unchanged. The asymmetric configuration is 0.12 eV lower in energy than the paraelectric phase, but the energy barrier for the H atom rotation is only 6 meV/unit cell (Fig. 2a). Due to the noncentrosymmetry of the structure, an out-of-plane macroscopic electric polarization is induced, which is 0.223×10^{-10}

C/m (2.06 μC/cm^2) from Berry phase calculations[42,43]. Such a value is larger than 1.60 μC/cm^2 in oxidized MXene[30], and an order of magnitude higher than 0.18 μC/cm^2 for the 1T phase of MoS$_2$[44]. Alternatively, when the H atom of hydroxide on the other side of the layer is rotated, the polarization direction is reversed (Fig.1c). Therefore, starting from the configuration in Fig. 1a with spontaneous polarization pointed upward (+P$_z$), one can switch off the polarization in an intermediate state (Fig. 1b) by rotating the H atom of hydroxide at the top of the layer after overcoming an energy barrier of 0.12 eV (Fig. 2a), then reverse the polarization to -P$_z$ by rotating the H atom of hydroxide on the other side of the layer. The electronic calculations for every image on the NEB path confirm that the structure remains fully gapped during the transition, thus ensuring a smooth polarization reversal as shown in Figure 2b.
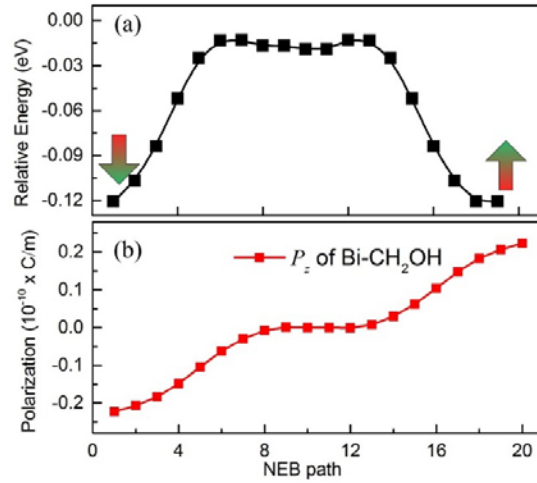

Figure 2. (a) Energy barriers for the ferroelectric switch and (b) the polarization variation along the path of the NEB calculations.

The electronic structures shown in Fig. 3a indicate that, the symmetric Bi-CH$_2$OH harbors the topological insulating order with an indirect band gap of 1.02 eV when the SOC is switched on as confirmed by Z$_2$ topological invariant calculations. Each SOC band is doubly degenerate because of the structural inversion symmetry. The large nontrivial band gap not only ensures the stable ferroelectricity, but also facilitates the observation of the QSH effect at room temperature. The non-SOC electronic properties are little changed as the spontaneous polarization persists along the z direction induced by the structural symmetry breaking. In contrast, on including the SOC, band degeneracies are lifted in the whole Brillouin zone since the frontier bands near the Fermi level are mainly from the p$_{x,y}$ orbit of Bi (see Fig. 5 in Appendix), which is sensitive to the out-of-plane polarization. As a result, a

characteristic Rashba-like band structure with an obvious Rashba splitting is seen, especially at the Γ and M points, and the band gap is reduced to 0.95 eV. Taken the conduction band minimum (CBM) at Γ as an example, the Rashba splitting E_R for the ferroelectric structure is 2 meV along Γ-M with a momentum offset of 0.011 Å^{-1}. The estimated Rashba parameter α_R= 0.364 eVÅ, it is comparable to that at Au surface[45] although smaller than the values for the bulk Rashba compound BiTeI [20]. Although the polarization induces an obvious spin splitting, the band topology is unchanged by the spontaneous polarization as confirmed by Z_2. The coexistence of ferroelectricity and band topology is therefore demonstrated in the same 2D material, namely the 2D FETI, for the first time.

To examine the effect of the ferroelectric switch on key electronic properties, we have presented the helical spin textures of the CBM states for $\pm P_z$ polarization. As seen in Fig. 3b, the valence and conduction bands are spin split and shifted in the k-space away from Γ point in the presence of SOC, therefore resulting in the inner and outer branches. The outer branch shows two symmetric energy minima, while the inner branch displays a cone shape (insert of Fig. 3b). These two split bands present nontrivial and opposite spin textures, with spins orthogonal to the crystal momenta. We have plotted the in-plane spin texture of the two CBM under $\pm P_z$ polarization where the direction of $S_{x,y}$ is indicated by arrows. Similar to FERSCs, the bands show the characteristic Rashba-like spin texture with the two bands having opposite spin orientations, with the inner band having a clockwise spin texture, while the outer band showing a counter-clockwise rotation of spins as one goes around the Brillouin zone centre. This spin texture can be reversed by switching the polarization, i.e., by rotating the atomic planes, as shown schematically in the figure. This result offers a feasible way to control and manipulate the spin texture in these materials.
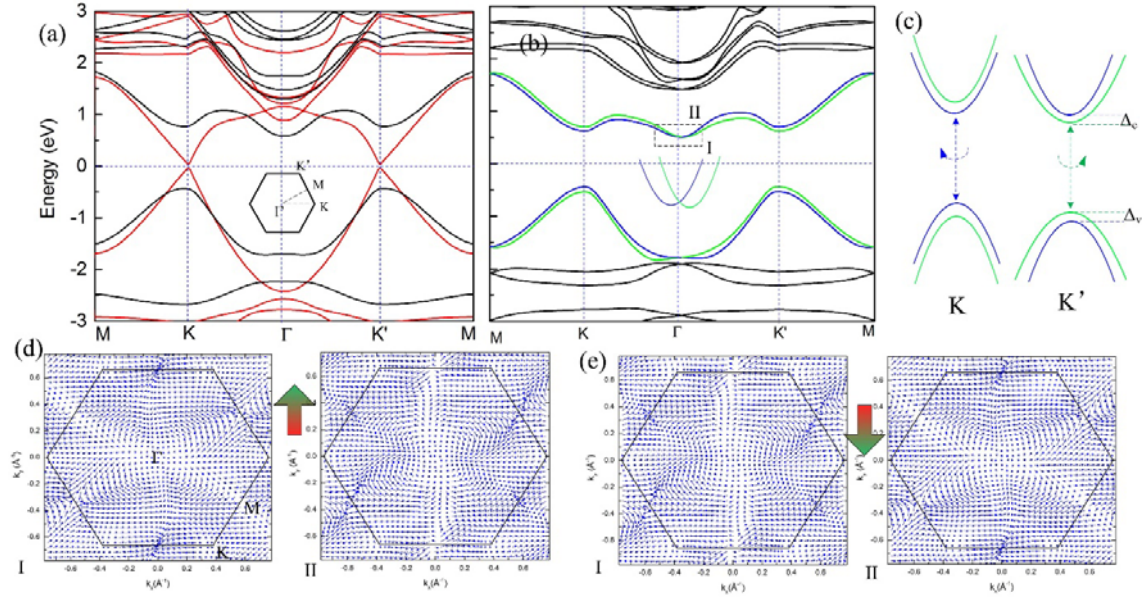
Figure 3. The band structures of Bi-CH$_2$OH without (red) and with (black) the SOC. (a) Results for the symmetric structure without out-of-plane polarization. (b) Results for the structure with +P$_z$ or -P$_z$ polarization, corresponding to the results shown in Figure 1a and 1c. The spin-up and down states are represented by the blue and green lines near the Fermi level, respectively. (c) Spin valley states at the K and K' points. (d, e) The in-plan spin textures of the conduction bands I and II shown in (b) under polarization +P$_z$ and -P$_z$.

Besides the spin texture reversal, ferroelectric switch also induces opposite sign spin splitting at the two non-equivalent K and K' points, leading to a spin valleytronic phenomena, similar to that in the MoS$_2$ [46,47]. We have distinguished the different spin states near Fermi level in Fig. 3b. It can be clearly seen that SOC splits the spin degeneracy of the CBM and VBM at the K and K' points owning to the absence of inversion symmetry, with the splitting of 72 meV (Δ_c) and 95 meV (Δ_v), respectively. The time reversal symmetry [E↑(k) = E↓(-k)] gives rise to the opposite ordering of the spin-up and spin-down states at the two inequivalent valley points, K and K'. Thus, the spin-up state at VBM/CBM at the K point is higher/lower than the spin-down state, while it is reversed at the K' point. As a result, the band gap at the K (K') point is dominated by the spin-up (spin-down) state. These two valleys therefore have opposite contributions to the quantum Hall conductivity, resulting in a quantum valley Hall (QVH) effect[16]. In contrast to the in-plane spin texture, such QVH effect is robust against the ferroelectric switch since the S$_z$ component is not significantly affected by the out-of-plane polarization.
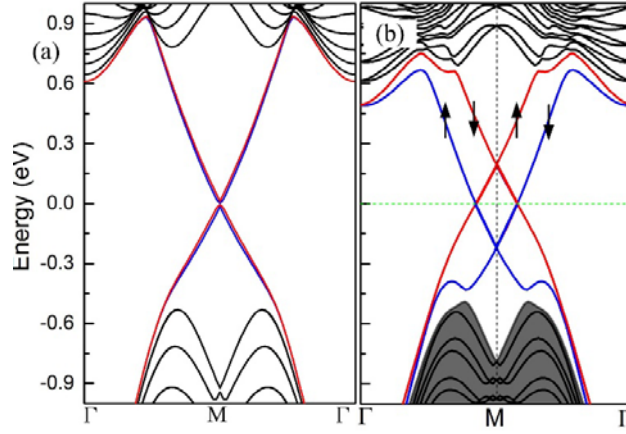
Figure 4. The edge states of (a) the symmetric configuration shown in Fig. 1b, and (b) the ferroelectrically ordered structure shown in Fig. 1a or 1c. The red and blues lines correspond to the edge state from the right and left sides, respectively, while the arrows indicate the spin-up or down states.

To calculate the edge states of the 2D FETI state, Bi-CH$_2$OH with zero and $\pm$P$_z$ polarization (i.e., the three configurations shown in Figure 1) are cut into 1D nanoribbons, with their edges passivated with hydrogen to remove the dangling bonds. The calculated results show that the metallic edge states characteristic of TIs are well preserved (Figure 4); however, there are some changes due to the presence of the ferroelectric order. Different from the degenerate states in the inversion symmetric structure without the out-of-plane polarization (Fig. 4a), the degeneracy of the edge states is lifted by the ferroelectric order, and the metallic states at two edges are split at the energies indicated by the red and blue lines in Fig. 4b.

Table 1. Summary of the functionalized Bi, Pb and Sb layers with ligand of -CH$_2$OH or –COOH, including the lattice constant a, energy barrier for ferroelectric switch E$_{barr}$, topological invariant Z$_2$, SOC gap E$_{g\_s}$ of the inversion symmetric structure, SOC gap E$_{g\_FE}$ of the asymmetric structure, the vertical polarization P$_z$, the Rashba parameter α_R of CBM at the Γ point, the splitting of CBM and VBM at the K point, Δ_c and Δ_v.

	a (Å)	E$_{barr}$ (eV)	Z$_2$	E$_{g\_s}$ (eV)	E$_{g\_FE}$ (eV)	P$_z$ (10^{-10} C/m)	α_R (eVÅ)	Δ_c (meV)	Δ_v (meV)
Bi-CH$_2$OH	5.497	0.12	1	1.02	0.95	0.223	0.364	72	95
Bi-COOH	5.497	0.452	1	1.0	0.917	0.204	0.472	26	74.2
Pb-CH$_2$OH	5.034	0.22	1	0.96	0.784	0.0263	0.737	61.2	25.3
Pb-COOH	5.034	0.548	1	0.924	0.67	0.2	1.269	80.3	148.9
Sb-CH$_2$OH	5.258	0.126	1	0.393	0.367	0.256	~0	41.5	41.2

To test the robustness of 2D FETIs, we examined other similarly constructed atomic thin layer structures. For Bi-COOH, the same coexisting multiple quantum orders are obtained as demonstrated by the results summarized in Table 1 and further supported by Fig. 6 in Appendix. Compared to Bi-CH$_2$OH, a significant Rashba effect (α_R=0.472 eVÅ) is obtained at the Γ point; however, the energy barrier to achieve the ferroelectric switch is at a higher value of 0.452 eV/unit cell. We also examined Pb/Sb-COOH or Pb/Sb-CH$_2$OH, as summarized in Table 1 and supported by Figures 7-10 in Appendix, these systems all belong to the same class of 2D FETIs. It should be mentioned that different from the functionalized Bi layer, the CBM and VBM are located around the Γ point for the functionalized Pb layers, and the resulting QVH effect at the K and K' points would be trivial since the gap is dominated by the states at the Γ point as indicated by Figure 8 in Appendix. However, the Rashba splitting at the Γ point are more pronounced than those in the Bi and Sb layers since the p$_{x,y}$ orbits of Pb near the Fermi level (Figure 9 in Appendix) can be considerably affected by the out-of-plane polarization when the inversion symmetry is broken. The Rashba parameter α_R of CBM for the nonsymmtric Pb-COOH is at a large value of 1.269 eVÅ, which is comparable to the result for BiTeI[19].

Our extensive calculations show that while details such as the values of the band gap and band splitting depend on the SOC strength of the specific element that makes up the atomic thin layers and also on the choice of the functional ligand groups, all the examined 2D FETIs possess the fundamental TI characteristics and reversible ferroelectric polarization. These findings indicate that coexisting TI and ferroelectric orders is a common phenomenon in these 2D layer systems. It is expected that the same strategy of looking for atomic thin layers of heavy elements like Bi, Pb and Sb functionalized by dipolar molecules like CH$_2$OCH$_3$, CH$_2$CHCH$_2$ and their variants can be expanded to other material systems of similar qualities, and their realization is feasible considering that CH$_2$OCH$_3$ or CH$_2$CHCH$_2$ functionalized germanene has been experimentally synthesized[40,41] and atomic thin Bi layer also has been experimentally obtained[14], which should facilitate the synthesis of 2D FETIs.

IV. Summary

In summary, we have introduced 2D FETIs as a new class of materials that exhibit coexisting ferroelectric and topological insulating orders. We have showcased the main characteristics of a prototype 2D FETI system in Bi-CH$_2$OH. Bi-CH$_2$OH exhibits a strong

topological insulating order in all the ferroelectric states, demonstrating a robust coexistence of the two distinct quantum orders in the same system. Furthermore, the interplay between the SOC and symmetry breaking leads to an additional spin valley phenomenon at the K and K' points and a strong Rashba splitting at the M and Γ points. These outstanding properties are also verified to be present in other similarly constructed 2D FETIs, and these remarkable quantum states of matter offer a unique platform for further exploration that may open new avenues leading to novel physics discoveries and innovative device applications.

APPENDIX: Stability of functionalized bismuthene, bandstrures and ferroelectricity of functionalized Bi, Pb and Sb layers

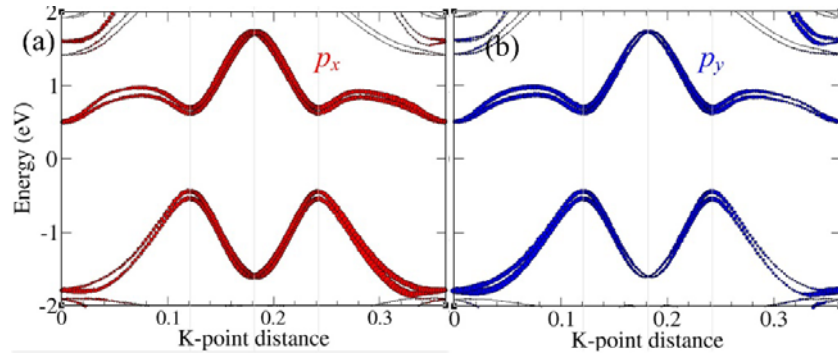Figure 5. Orbital resolved band structure of CH$_2$OH functionalized bismuthene with the polarization of $\pm$Pz, where the red and blue dots represent the states of px and py of Bi, respectively.
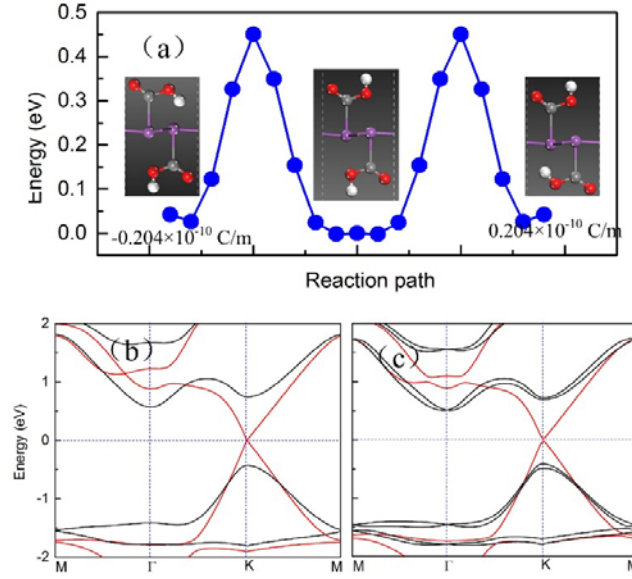
Figure 6. (a) Energy barriers for the ferroelectric switch in Bi-COOH. The structures of three key symmetric and nonsymmetric Bi-COOH configurations are shown. Electronic band structures of the Bi-COOH layer the SOC off (red) and on (blue) for the structures without (b) and with (c) the out-of-plane polarization. The band topology is preserved throughout the polarization switch process as verified by Z_2 calculations, with the nontrivial indirect gap of 1.0 eV (0.917 eV) for symmetric (nonsymmetric) configurations. The vertical polarization is calculated to be 0.204×10^{-10} C/m. The blue and green colors near the Fermi level indicate the spin-up and down state, respectively.
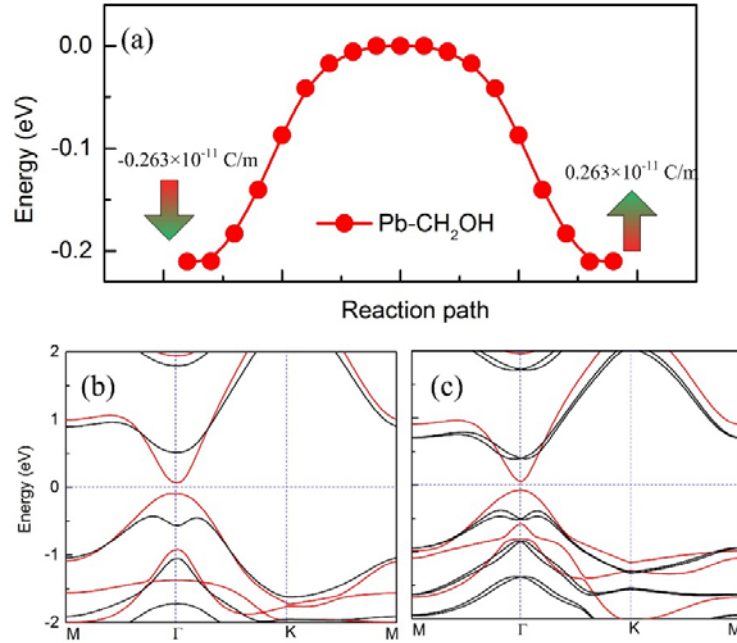

Figure 7. (a) The energy barrier for the ferroelectric switch of Pb-CH$_2$OH; (b, c) Electronic band structures of Pb-CH$_2$OH with the SOC off (red) and on (black). The vertical polarization is calculated to be 0.263×10^{-11} C/m when the inversion symmetry is broken. The band topology is preserved with the nontrivial indirect gap of 0.96 eV (0.784 eV) for the symmetric (nonsymmetric) configurations.
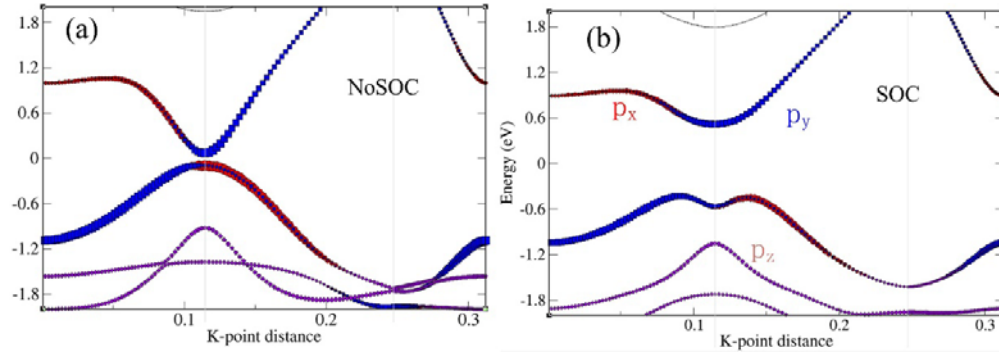
Figure 8. Orbital resolved band structures of Pb-CH$_2$OH layer the SOC off (a) and on (b). Here px, py and pz are indicated by red, blue and pink colors, respectively. One can see the band switch between px and py after the SOC is turned on.
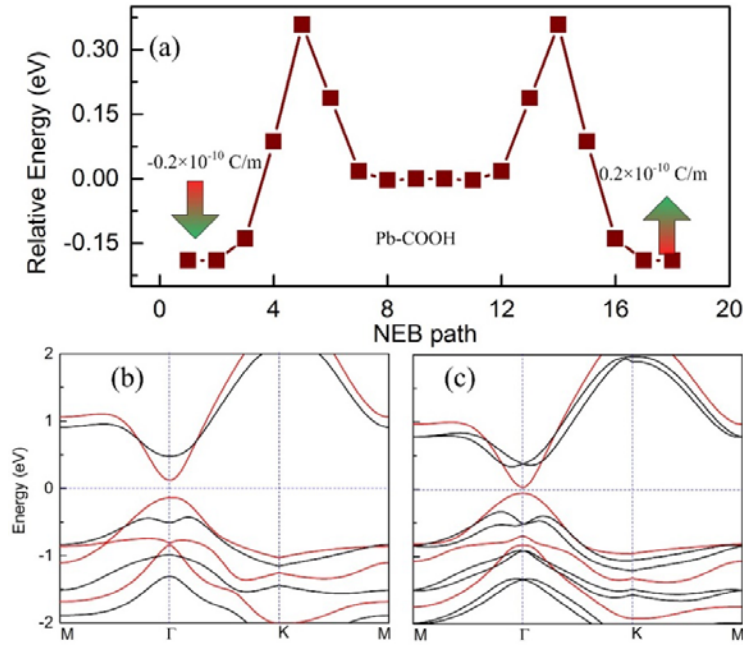

Figure 9. (a) Energy barriers for the ferroelectric switch of Pb-COOH; (b, c) Electronic band structures of Pb-COOH with the SOC off (red) and on (black). The vertical polarization is calculated to be 0.2×10^{-10} C/m when the inversion symmetry is broken. The band topology is preserved with the nontrivial indirect gap of 0.96 eV (0.784 eV) for symmetric (nonsymmetric) configurations.
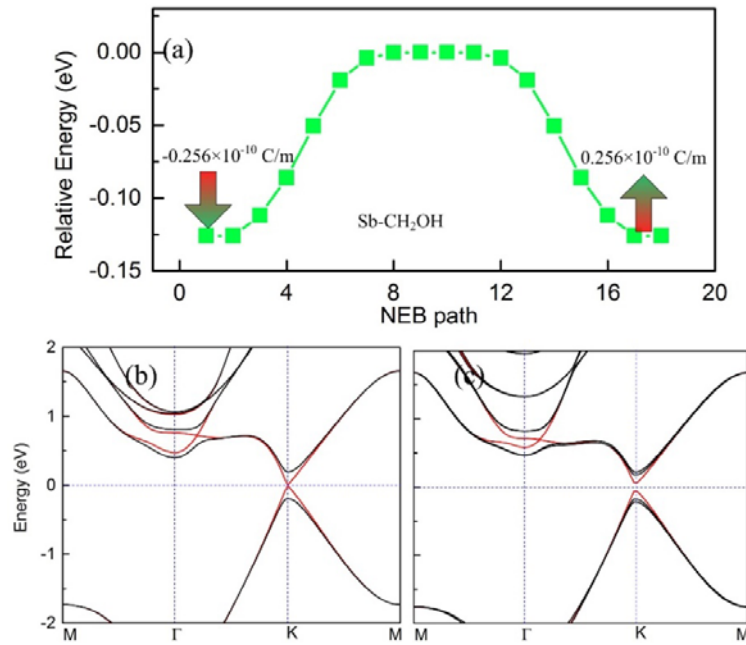
Figure 10. (a) The energy barrier for the ferroelectric switch of Sb-CH$_2$OH; (b,c) Electronic band structures of Sb-CH$_2$OH with the SOC off (red) and on (black). The vertical polarization is calculated to be 0.256×10^{-10} C/m when the inversion symmetry is broken.

References

[1]   X.-L. Qi and S.-C. Zhang, Reviews of Modern Physics **83**, 1057 (2011).
[2]   M. Z. Hasan and C. L. Kane, Reviews of Modern Physics **82**, 3045 (2010).
[3]   Y. Binghai and Z. Shou-Cheng, Reports on Progress in Physics **75**, 096501 (2012).
[4]   J. Wunderlich, B.-G. Park, A. C. Irvine, L. P. Zârbo, E. Rozkotová, P. Nemec, V. Novák, J. Sinova, and T. Jungwirth, Science **330**, 1801 (2010).
[5]   L. Kou, Y. Ma, Z. Sun, T. Heine, and C. Chen, The Journal of Physical Chemistry Letters **8**, 1905 (2017).
[6]   F.-C. Chuang, L.-Z. Yao, Z.-Q. Huang, Y.-T. Liu, C.-H. Hsu, T. Das, H. Lin, and A. Bansil, Nano Letters **14**, 2505 (2014).
[7]   C. P. Crisostomo, L.-Z. Yao, Z.-Q. Huang, C.-H. Hsu, F.-C. Chuang, H. Lin, M. A. Albao, and A. Bansil, Nano Letters **15**, 6568 (2015).
[8]   L. Kou, B. Yan, F. Hu, S. C. Wu, T. O. Wehling, C. Felser, C. Chen, and T. Frauenheim, Nano Letters **13**, 6251 (2013).
[9]   W. Luo and H. Xiang, Nano Letters **15**, 3230 (2015).
[10]   Y. Ma, Y. Dai, L. Kou, T. Frauenheim, and T. Heine, Nano Letters **15**, 1083 (2015).
[11]   M. König, S. Wiedmann, C. Brüne, A. Roth, H. Buhmann, L. W. Molenkamp, X.-L. Qi, and S.-C. Zhang, Science **318**, 766 (2007).
[12]   Y. Xu, B. Yan, H.-J. Zhang, J. Wang, G. Xu, P. Tang, W. Duan, and S.-C. Zhang, Physical Review Letters **111**, 136804 (2013).
[13]   F.-f. Zhu, W.-j. Chen, Y. Xu, C.-l. Gao, D.-d. Guan, C.-h. Liu, D. Qian, S.-C. Zhang, and J.-f. Jia, Nat Mater **14**, 1020 (2015).
[14]   F. Reis, G. Li, L. Dudy, M. Bauernfeind, S. Glass, W. Hanke, R. Thomale, J. Schäfer, and R. Claessen, Science (2017).
[15]   M. S. Bahramy, B. J. Yang, R. Arita, and N. Nagaosa, Nat Commun **3**, 679 (2012).
[16]   A. Manchon, H. C. Koo, J. Nitta, S. M. Frolov, and R. A. Duine, Nat Mater **14**, 871 (2015).
[17]   G. Dresselhaus, Physical Review **100**, 580 (1955).

[18]   J. Nitta, T. Akazaki, H. Takayanagi, and T. Enoki, Physical Review Letters **78**, 1335 (1997).

[19]   K. Ishizaka *et al.*, Nat Mater **10**, 521 (2011).

[20]   H. Maass *et al.*, Nat Commun **7**, 11621 (2016).

[21]   A. Narayan, Physical Review B **92**, 220101 (2015).

[22]   D. Di Sante, P. Barone, R. Bertacco, and S. Picozzi, Advanced Materials **25**, 509 (2013).

[23]   D. Di Sante, P. Barone, A. Stroppa, K. F. Garrity, D. Vanderbilt, and S. Picozzi, Physical Review Letters **117**, 076401 (2016).

[24]   P. Z. Hanakata, A. S. Rodin, A. Carvalho, H. S. Park, D. K. Campbell, and A. H. Castro Neto, Physical Review B **96**, 161401 (2017).

[25]   D. Di Sante, A. Stroppa, P. Barone, M.-H. Whangbo, and S. Picozzi, Physical Review B **91**, 161401 (2015).

[26]   A. Stroppa, D. Di Sante, P. Barone, M. Bokdam, G. Kresse, C. Franchini, M. H. Whangbo, and S. Picozzi, Nat Commun **5**, 5900 (2014).

[27]   S. Picozzi, Frontiers in Physics **2** (2014).

[28]   B. Monserrat, J. W. Bennett, K. M. Rabe, and D. Vanderbilt, Physical Review Letters **119**, 036802 (2017).

[29]   S. Liu, Y. Kim, L. Z. Tan, and A. M. Rappe, Nano Letters **16**, 1663 (2016).

[30]   A. Chandrasekaran, A. Mishra, and A. K. Singh, Nano Letters **17**, 3290 (2017).

[31]   M. Wu and X. C. Zeng, Nano Letters **16**, 3236 (2016).

[32]   W. Ding, J. Zhu, Z. Wang, Y. Gao, D. Xiao, Y. Gu, Z. Zhang, and W. Zhu, **8**, 14956 (2017).

[33]   M. Wu, S. Dong, K. Yao, J. Liu, and X. C. Zeng, Nano Letters **16**, 7309 (2016).

[34]   G. Kresse and J. Furthmüller, Physical Review B **54**, 11169 (1996).

[35]   J. P. Perdew, K. Burke, and M. Ernzerhof, Physical Review Letters **77**, 3865 (1996).

[36]   S. Grimme, Journal of Computational Chemistry **27**, 1787 (2006).

[37]   The Journal of Chemical Physics **113**, 9901 (2000).

[38]   Z. Song *et al.*, NPG Asia Mater **6**, e147 (2014).

[39]   J. W. Bennett, I. Grinberg, and A. M. Rappe, Journal of the American Chemical Society **130**, 17409 (2008).

[40]   S. Jiang *et al.*, Chemistry of Materials **28**, 8071 (2016).

[41]   S. Jiang, S. Butler, E. Bianco, O. D. Restrepo, W. Windl, and J. E. Goldberger, **5**, 3389 (2014).

[42]   R. Resta and D. Vanderbilt, in *Physics of Ferroelectrics: A Modern Perspective* (Springer Berlin Heidelberg, Berlin, Heidelberg, 2007), pp. 31.

[43]   R. Resta, Europhysics News **28**, 18 (1997).

[44]   S. N. Shirodkar and U. V. Waghmare, Physical Review Letters **112**, 157601 (2014).

[45]   S. LaShell, B. A. McDougall, and E. Jensen, Physical Review Letters **77**, 3419 (1996).

[46]   SuzukiR *et al.*, Nat Nano **9**, 611 (2014).

[47]   D. Xiao, G.-B. Liu, W. Feng, X. Xu, and W. Yao, Physical Review Letters **108**, 196802 (2012).